PAPER

Check for updates

Large-scale fabrication of waterborne superamphiphobic coatings for flexible applications†

Youfa Zhang, ID *[a] Daozhou Yao,[a] Shanlin Wang,[b] Zhen Xiao[a] and Xinquan Yu[a]

In recent years, there have been great achievements in superhydrophobic coatings. However, there are still some barriers restricting superhydrophobic coatings in practical applications, such as widely used organic solvents and poor oleophobicity. In this study, we proposed a method for fabricating absolutely waterborne superamphiphobic coatings in two steps. Firstly, we synthesized the waterborne SiO_2 sol using methyltriethoxysilane, and then the SiO_2 sol was modified in an aqueous system with a fluorocarbon surfactant. The results showed that the coating had contact angles of 160°, 153° and 150° and sliding angles of 1°, 4.7° and 6.3° with respect to water, soybean oil and hexadecane. Moreover, the coating could withstand 300 °C heating and immersion in various corrosive solutions for several hours. Furthermore, it is worth mentioning that the waterborne coating showed excellent performances in antifouling, self-cleaning, and damp-proof fields.

1 Introduction

The demand for water repellent and antifouling properties has been increasing gradually owing to severer and severer environmental problems.[1–3] Inspired by the lotus leaf, superhydrophobic surfaces, having a greater water contact angle (CA) than 150° and a lower sliding angle (SA) than 10°, were proposed in an attempt to satisfy the aforementioned demand. To our delight, superhydrophobic surfaces have tremendous potential applications in self-cleaning,[4–7] anti-icing,[8–13] drag reduction,[14–16] water–oil separation[17–22] and atmospheric water capture.[23–25] However, the superhydrophobic surfaces tend to lose their effects when exposed to external environments for a long time due to the presence of various organic contaminants, to a great extent. As a consequence, the question of how to improve the durability of superhydrophobic surfaces after long-term exposure to the outside has drawn the attention of researchers. Superamphiphobic surfaces, with both superhydrophobicity and superoleophobicity, are very desirable due to the fact that they are promising for solving the problems above. Nevertheless, it is much harder to fabricate superamphiphobic surfaces, which possess larger roughness and lower surface free energy. Several methods have been proposed

to prepare superamphiphobic surfaces, such as functionalization with nanoparticles,[26] etching,[27,28] lithography,[29] template-assisted synthesis[5] and sol–gel routes.[30] Recently, Susarrey-Arce and his coworkers[31] developed a method to fabricate arrays of microstructures *via* the reactive ion etching of a silicon wafer, which was covered by a patterned photoresist layer. Regrettably, it seems that with this method it was difficult to fabricate superamphiphobic surfaces on a large scale because of the complex process and costly equipment. Among various methods, wet-chemical processes by dip-coating or spraying are the focus of concern due to their great convenience for large-scale fabricating with a low reliance on equipment.

To the best of our knowledge, most of the solvents that are used in the wet-chemical systems are organic, including ethanol,[32] acetone,[33] dimethylformamide (DMF),[33] and tetrahydrofuran (THF),[34] which are considered to be harmful to both the environment and human health. Consequently, it is impossible to prepare superamphiphobic coatings consisting of an organic solvent on a large scale. Water, known as a green and cost-effective solvent, is of great interest to scientists around the world. In recent years, Bayer and co-workers[35] have reported the formation of a superamphiphobic surface through spraying an aqueous solution consisting of spherical and porous silicon dioxide nanopowder, hydrophilic fumed silica and waterborne acrylic fluorochemical dispersion on high temperature metallic substrates. However, most of the reported waterborne superamphiphobic coatings have an inaccessible preparation cost, restricting their further practical application.

Herein, we developed a simple, low-cost, environmentally friendly method to fabricate waterborne superamphiphobic coatings using methyltriethoxysilane, fluorinated alkyl silane

[a]*Jiangsu Key Laboratory of Advanced Metallic Materials, School of Materials Science and Engineering, Southeast University, Nanjing 211189, P. R. China. E-mail: yfzhang@seu.edu.cn*

[b]*School of Material Science and Engineering, Southwest University of Science and Technology, Mianyang 621010, PR China*

and a fluorocarbon surfactant as the principal raw materials. Firstly, waterborne SiO$_2$ sol was synthesized *via* a hydrolysis process of methyltriethoxysilane in water. The following step was the modification of the SiO$_2$ sol through fluorinated alkyl silane in water with a fluorocarbon surfactant. Subsequently, the superamphiphobic coatings were prepared by spraying or dip-coating on glass, polyester fiber, copper foam and some other substrates. The coating showed an excellent super-amphiphobic ability with contact angles of 160°, 153° and 150° and sliding angles of 1°, 4.7° and 6.3° with respect to water, soybean oil and hexadecane. Furthermore, the coating could be coated on various substrate surfaces, such as glass, copper foam and polyester fiber, it performed very well in terms of chemical durability and thermal stability and it has potential for practical use in antifouling, self-cleaning and damp-proof fields.

2   Materials and methods

2.1   Materials

Methyltriethoxysilane (MTES) was purchased from Tokyo Chemical Industry Co, Ltd. ForaperLe 323 (FL323) fluorocarbon surfactant was supplied by DuPont. 1*H*,1*H*,2*H*,2*H*-Peruor-odecyltriethoxysilane (PFDTES) was purchased from Sikang New Material Co., Ltd. Tetraethoxysilane (TEOS), sodium dodecyl benzene sulfonate (SDBS), deionized water, ammonia solution (NH$_3$·H$_2$O, 28 wt%) and other chemical reagents were purchased from Sinopharm Chemical Reagent Co., Ltd.

2.2   Synthesis of waterborne SiO$_2$ sol

Firstly, 0.2 g SDBS, 2 mL NH$_3$·H$_2$O and 36 g deionized water were mixed homogeneously *via* magnetic stirring for 15 min. Then, 15.2 g methyltriethoxysilane was added to the solution dropwise. Subsequently, the mixed solution was left to stir at 60 °C for 12 to 60 hours to obtain waterborne SiO$_2$ sol.

2.3   Fabrication of the waterborne coatings

First of all, 12.5 g fluorocarbon surfactant and 30 g SiO$_2$ sol were added to 2 L deionized water with 100 mL NH$_3$·H$_2$O in it. After magnetic stirring for 10 min, 15 mL TEOS was added. Subsequently, 15 mL PFDTES was added dropwise to the system. The mentioned solution was left to stir at 600 rpm at 45 °C for 24 h to fabricate the waterborne coatings.

2.4   Characterizations

The microstructure of the sample surface was observed using field emission scanning electron microscopy (FESEM) and transmission electron microscopy (TEM). Static contact angles (CA) and sliding angles (SA) were determined at room temperature using an OCA 15 Pro contact angle meter to characterize the hydrophobicity of the specimens. The average CA values were determined by measuring the same sample at 3–5 different positions. The volume of the water droplet was 5 μL for CA and 10 μL for SA unless noted otherwise. The water droplet bouncing test was captured using a Photron FASTCAM Mini UX100 type high speed camera equipped with a Navitar 6000 zoom lens. The particle size distribution of the waterborne

coatings and the infrared spectrogram of the SiO$_2$ sol were measured using a Laser Particle Size Analyzer using Microtrac S3500 and Fourier transform infrared spectroscopy using Nicolet 5700. All the coatings were prepared by spraying or dip-coating using an airbrush (S-130, U-STAR) and padder (made by ourselves, for the purpose of squeezing extra liquids in fiber).

3   Results and discussions

3.1   Preparation of the waterborne coatings

The waterborne superamphiphobic coatings were prepared *via* a modified reaction between the SiO$_2$ sol and 1*H*,1*H*,2*H*,2*H*-perfluorodecyltrichlorosilane (PFDTES), and the schematic for this is shown in Fig. 1a. First of all, SiO$_2$ sol was synthesized using methyltriethoxysilane (MTES). The MTES was hydrolyzed in an aqueous system and sodium dodecyl benzene sulfonate (SDBS) was used to promote the solubility of MTES in water. The finally prepared SiO$_2$ sol is shown in Fig. S1.† It is apparent from the optical photograph that the synthesized SiO$_2$ sol was milky. In addition, we found that the hydrolysis time for methyl-triethoxysilane was an important factor for controlling the SiO$_2$ sol morphology. Fig. S2† shows the TEM images of the SiO$_2$ sol with different hydrolysis times from 12 h to 60 h. As the TEM images show, the diameter of the SiO$_2$ particles was about 30 nm regardless of the hydrolysis time, but a difference lay in the extent of the polycondensation between the SiO$_2$ particles. When the reaction was allowed to occur for 12 h, the extent of the polycondensation of the SiO$_2$ particles was relatively low and there was a large gap between the particles. The opposite was the case when the hydrolysis time was 60 h. Based on the above results, the determined hydrolysis time was 36 h, which was considered to be the optimum time for preparing the SiO$_2$ sol, and all of the samples mentioned later were fabricated using SiO$_2$ sol that was reacted for 36 h unless noted otherwise. Subsequently, the as-prepared SiO$_2$ sol and the ForaperLe 323 (FL323) (which is a kind of fluorocarbon surfactant consisting of a waterborne acrylic fluoropolymer) were well-dispersed in an alkaline aqueous system. Tetraethoxysilane (TEOS) and PFDTES were added in the following step. After constant stirring for 24 h, the preparation process was finished. Changes to the chemical bonding during fabrication are shown in Fig. S3.† The inset optical image in Fig. 1b is a photograph of the as-prepared waterborne paint, indicating that the solution was semi-transparent. The dynamic light scattering (DLS) measurements shown in Fig. 1b revealed that the average diameter of the waterborne paint was approximately 660 nm. The most positive aspect was that the waterborne superamphiphobic paint could be prepared on a large scale (Fig. S4†) with an acceptable cost, which can be seen as a breakthrough in the application fields of waterborne superamphiphobic coatings. Fig. 1c shows the FTIR spectra of the as-prepared SiO$_2$ sol and coating, indicating that the SiO$_2$ sol was successfully modified by PFDTES in the aqueous system. For the SiO$_2$ sol, the asymmetric stretching vibration of Si–O–Si gave strong absorption peaks at 1033 cm^{-1} and 1120 cm^{-1}. The absorption peak at 782 cm^{-1} can be assigned to the presence of Si–C bonds, while the strong bands at 1409 cm^{-1}, 2935 cm^{-1} and 2973 cm^{-1} can
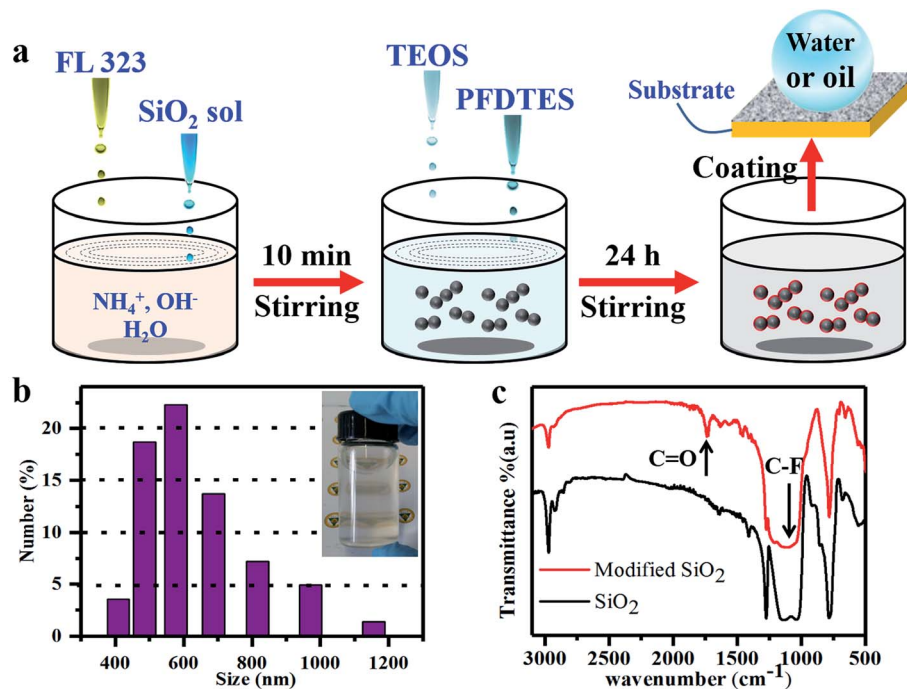
Fig. 1 Preparation of the waterborne superamphiphobic coating. (a) Schematic of the fabrication of the superamphiphobic coating. (b) Size distribution in the waterborne superamphiphobic paint (inset: photograph of the waterborne superamphiphobic paint in a transparent glass bottle). (c) FTIR spectra of the SiO_2 sol and the waterborne superamphiphobic coating (all the samples were dried into a powder at 80 °C to test FTIR).

be attributed to the asymmetrical stretching of the $-CH_3$ groups. After being modified, the FTIR spectra sketch of SiO_2 had a significant change. Apart from the absorption peaks attributed to SiO_2 that were mentioned before, the modified SiO_2 had a new absorption peak at 1725 cm^{-1}, which can be assigned to the symmetric stretching vibration of C=O in the fluorocarbon surfactant. As we know, the characteristic peaks of the various stretching vibrations of $-CF_2$ and $-CF_3$ are at 1121, 1145, 1198, and 1241 cm^{-1}, which are very close to the asymmetric stretching vibrations of Si–O–Si at 1033 cm^{-1} and 1120 cm^{-1}. As a consequence, the width of the absorption peak was enlarged distinctly.

3.2 Effect of the hydrolysis time for methyltriethoxysilane on the coating

As mentioned before, the hydrolysis time of methyltriethoxysilane had an important effect on the SiO_2 sol morphology, which is considered to be one of the principal factors in preparing superamphiphobic surfaces. As Fig. 2a shows, with the changing hydrolysis time, the coatings were all super-repellent to water (surface tension: 72.1 mN m^{-1}) and soybean oil (35.7 mN m^{-1}), but only a few coatings were super-repellent to hexadecane (27.5 mN m^{-1}). When the hydrolysis time for methyltriethoxysilane was 36 h, the coating had a maximum contact angle (150°) and minimum sliding angle (6.3°) to hexadecane, indicating that this coating had the best superamphiphobicity. The reason for this lies in the final morphology of the coatings, and scanning electron microscopy (SEM) images are shown in Fig. 2b–d. Compared to the other

two coatings (where the hydrolysis time of methyltriethoxysilane is 12 h (Fig. 2b) and 60 h (Fig. 2d)), the coating prepared using the SiO_2 sol that was hydrolyzed for 36 h (Fig. 2c) had a more compact and uniform morphology at the micro-scale. Furthermore, the network structure in Fig. 2c had fewer microholes than the two other coatings did. A similar case appeared when the magnification times were enlarged at the nano-scale. The coating with the SiO_2 that had reacted for 36 h had more roughness to its structure and the nanoparticles in this sample were denser than they were in the two other coatings. The dense and uniform micro-nano structure resulted in better repellency of hexadecane. The fracture surface morphology of the superamphiphobic coating is presented in Fig. S5† and the upside-down circular truncated cone structure (which was called the "reentrant structure") could be seen clearly, resulting in the superamphiphobicity of our prepared coating.

3.3 Applicability of the waterborne coatings on various substrates

In order to test the superamphiphobicity on various substrates, three typical materials were selected: flat (glass), porous (copper foam) and soft (polyester fiber) substrates. As showed in the left position of Fig. 3a–c, all three substrates revealed excellent superhydrophobicity and there was no distinct change in the original state of the substrates after being coated. For example, the coated glass was translucent and we could see the badge beneath the substrates clearly. The water and oil contact angles and sliding angles are presented in Fig. S6.† For the contact
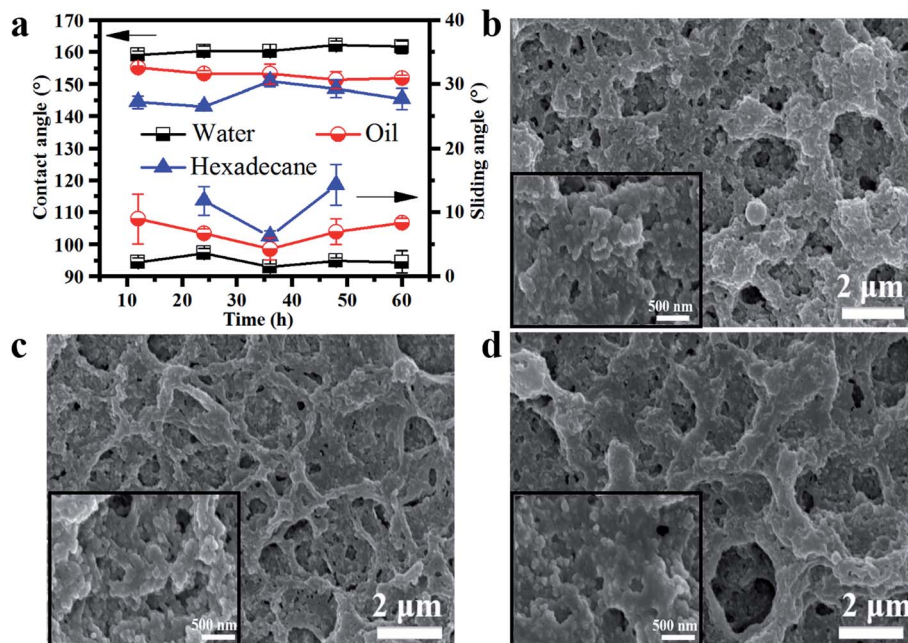
Fig. 2 (a) Contact angles and sliding angles of water, oil and hexadecane on the waterborne coating with different hydrolysis times of methyltriethoxysilane. SEM images of the waterborne coatings with hydrolysis times of methyltriethoxysilane of (b) 12 h, (c) 36 h and (d) 60 h.

angle values, these were about 160° and 153° for water and oil, respectively. For the sliding angle values, the values for glass and copper foam were all below 10° for both water and oil. However, for fiber, the sliding angle was relatively large (15° and 37° for water and oil, respectively) due to the coarser texture of the fiber resulting in strong adhesion between the substrate and the liquid drop. When the volume of tested liquid (water and oil) was set at 25 μL, the sliding angle values decreased sharply

to 7° and 16° for water and oil, respectively. We also chose some commercial fabrics to test and both showed an excellent superamphiphobicity (Fig. S7†). Based on the results above, we believe that the waterborne coating has an outstanding applicability on various substrates (for more details, see Video S1†).

The middle position of Fig. 3a–c shows the SEM images of the different substrates (the original morphologies of the copper foam and polyester fiber are listed in Fig. S8†) after
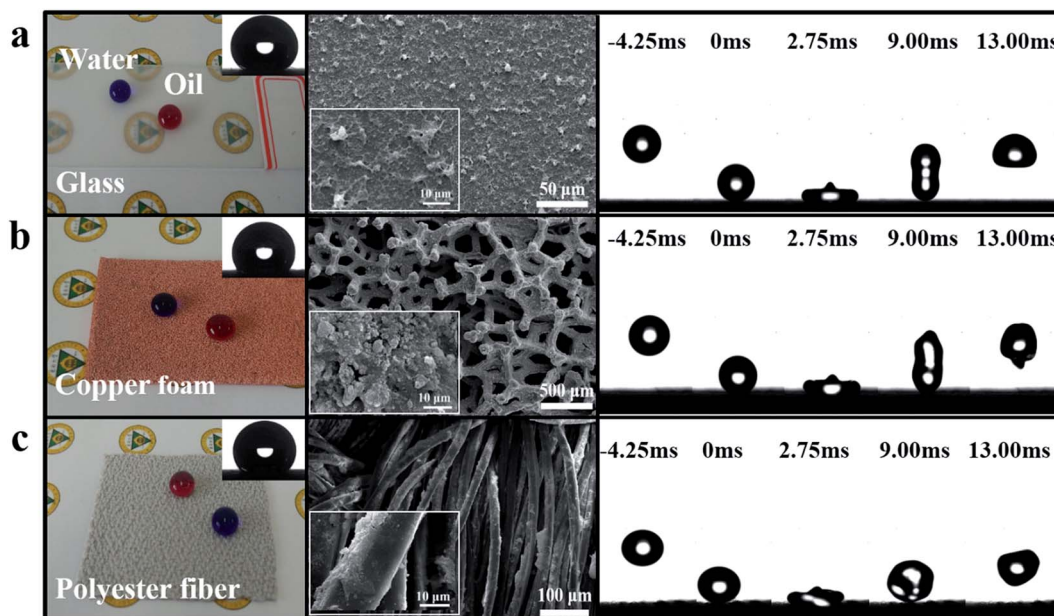

Fig. 3 Photographs (left, inset: oil contact angle images), SEM images (middle) and impacting test results (right, with a volume of 5 μL and a height of 15 mm between the water droplet and the substrate) on (a) glass, (b) copper foam and (c) polyester fiber substrates.

being coated with the waterborne paints, showing the textured surface morphologies for each one. The right position shows the high speed camera images of the bouncing water droplets on the various substrates (the height between the water drop and the substrate was 15 mm, and the volume of water was 5 μL). The water droplets could completely leave the surface without wetting, penetrating or damaging it for both the hard and soft substrates, showing that water has an extremely low adhesion with the various substrates. Based on the facts above, we believe that the coatings could stabilize on different substrates through the spraying or dip-coating method.[36,37]

3.4 Thermal stability

It was unknown whether the as-prepared coatings could remain superamphiphobic under high temperature. Therefore, the water and oil contact angles and sliding angles under temperatures ranging from 100 °C to 300 °C were investigated to evaluate the thermal stability of the coating. As shown in Fig. 4a, when the temperature was below 200 °C, the coating still remained superamphiphobic and there was no visible change in the water and oil contact angles and sliding angles. However, the coating became oleophilic and superoleophilic when the temperature increased to 250 °C and 300 °C, respectively, while it remained as superhydrophobic as before. However, the coating was still superamphiphobic after 150 °C heating for 48 h (Fig. S9†).

It was interesting that the coating treated at 300 °C (which was superhydrophobic and superoleophilic) returned to being superamphiphobic after being deposited in a layer of PFDTES (namely the fluorination mentioned in Fig. 4b). Based on the results above, we believed that the coating becoming

superoleophilic was attributed to the degradation of the substance containing the F element. SEM images and energy dispersive spectrometry (EDS) were measured to prove this point. As shown in Fig. 4c and d, the structure of the as-prepared coating and the coating treated at 300 °C had little change, but the content of the F and C elements decreased sharply, while there was no obvious change in the content of Si after treating at 300 °C (the whole EDS is listed in Fig. S10†), indicating that the fluorocarbon surfactant degraded during the heating process.

3.5 Chemical durability

In addition to high temperature, the superamphiphobicity of coatings tends to recede when they are exposed to corrosive environments such as strong acid, base and high salt spray. Herein, we put the coated glasses into different pH values from 1 to 13 and into 1 mol L^{-1} NaCl solutions and immersed them for 2 h to test the chemical durability of the coatings. Fig. S11a† shows digital photographs of the coatings that were immersed in different corrosive solutions and after immersing for 2 h, revealing that the surfaces were all clean and there were no residual liquids on the coated glasses. More importantly, the coated glasses could keep clean even when immersed in oil after 2 h of immersion in different corrosive solutions (Fig. S11b†). The water and oil contact angle and sliding angle values are listed in Fig. 5a and b. As the results show, the contact angle values were all close to 160° and 150° and the sliding angle values were still below 10° and 15° for water and oil, respectively. In other words, the coating could withstand different corrosive environments for a certain time.
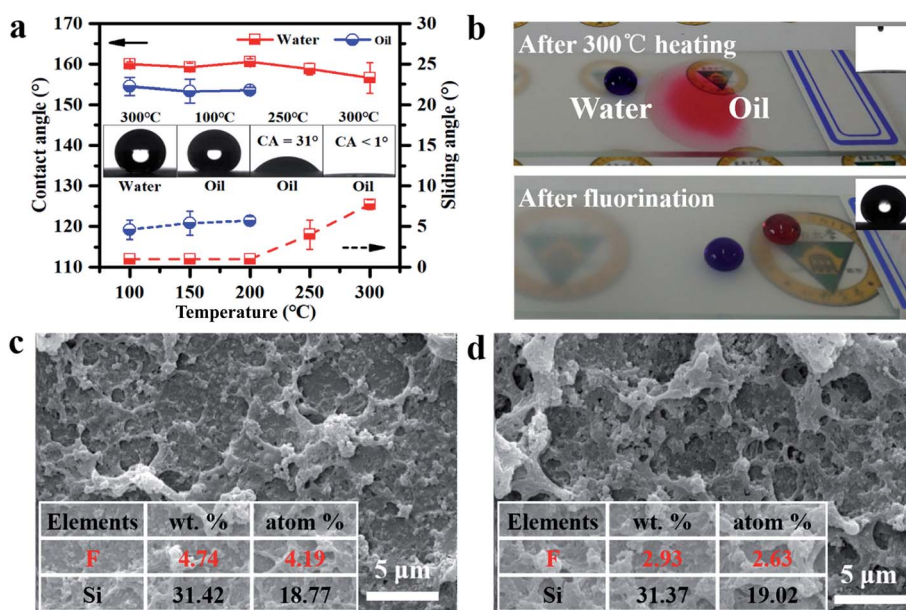

Fig. 4 Thermal stability of the coating. (a) Change in the contact angles and sliding angles (water and oil) with the temperature increasing from 100 °C to 300 °C for 2 h (inset: water and oil contact angle images). (b) Optical photographs of the coating on the glass substrate after 300 °C heating and after fluorination (inset: oil contact angle images). SEM images before 300 °C heating (c) and after heating (d) (inset table: content of F and Si elements).
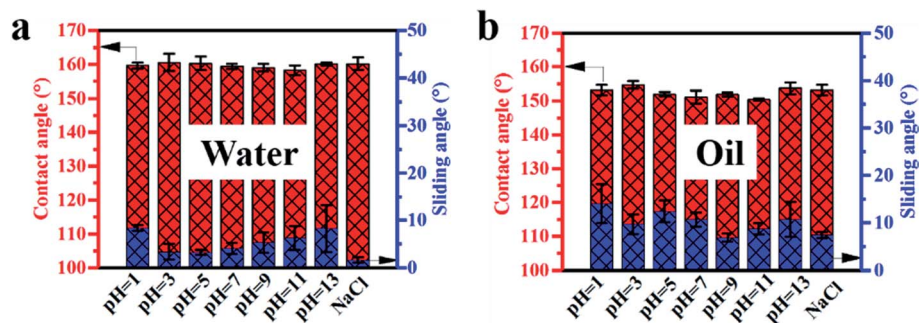
Fig. 5 Change in the contact angles and sliding angles for water (a) and oil (b) in different corrosive solutions after immersing for 2 h.

3.6 Applications of the waterborne coating

Antifouling and self-cleaning properties. As we know, superhydrophobic surfaces can always remain clean under various conditions because of self-cleaning effects. Nevertheless, whether the surfaces can still remain clean under the severe conditions contained in oil fouling has rarely been reported.

We chose a glove and dyed water and oil to test the antifouling properties. The index finger of the glove was treated with the coating and the middle finger was untreated, as shown in Fig. S12a.† Then the two fingers were immersed in the dyed oil simultaneously for several minutes. After being taken out, the index finger didn't have any oil stains on it while the middle finger was wetted by the dyed oil completely. Even after bending several times, the index finger could still remain completely clean. Based on the results above, we are convinced that the waterborne coating is able to be qualified in the antifouling field under most conditions. As for the self-cleaning properties

test, ordinary sludge powder and sludge powder containing oil fouling were used to simulate a complex environment. As shown in Fig. S12b,† the as-prepared coating exhibits excellent self-cleaning properties and water (dyed blue) can roll-off from the surface without a hitch, and as a result of which, the sludge powder can be taken away (for more details, see Video S2†). When the sludge powder containing oil fouling (a mixture of edible oil and sludge powder) was used, the mixture could also slide from the surfaces (Video S3†). In the end, there was no residue on the surfaces, indicating that the coatings have excellent self-cleaning properties under various complicated conditions.

Damp-proof testing on polyester fiber. Fibers tend to go mouldy when they are in a humid environment, and as a result of which, damp-proof properties are one of the most primary demands for various fibers. It is universally acknowledged that superhydrophobic surfaces have an excellent performance in the water-proof field. However, it remains in doubt whether all
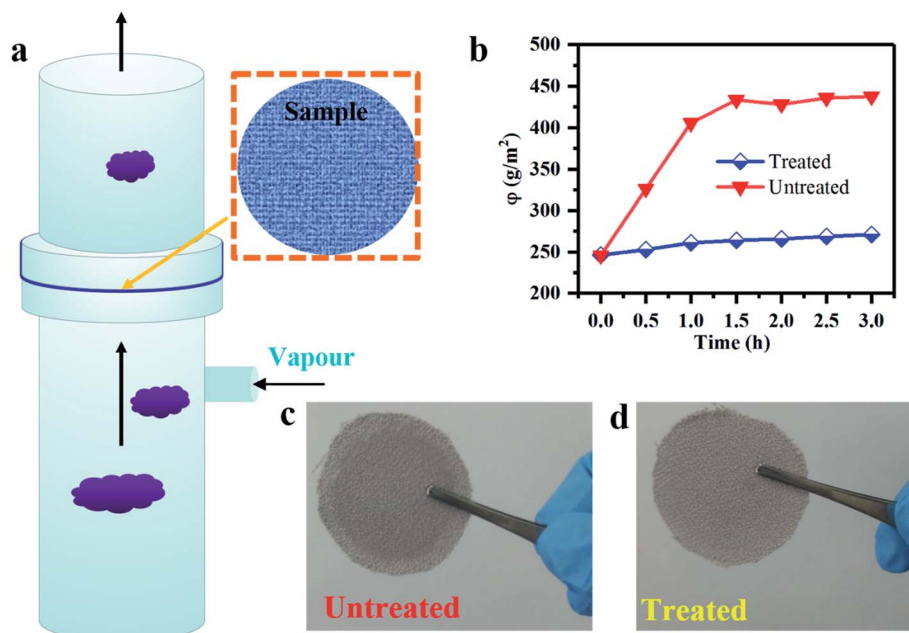

Fig. 6 Damp-proof test on polyester fiber. (a) Schematic of the damp-proof test. (b) Unit area mass change of the treated and untreated fibers at a certain humidity. Photograph of the untreated fiber (c) and treated fiber (d).

superhydrophobic surfaces are capable in humid environments. Fig. 6a shows the schematic of the damp-proof test, in which two glass tubes and a humidifier were used. The samples were fixed between the two glass tubes (detailed data of the samples and glass tubes are listed in Fig. S13†) and the dampness was brought in from below and allowed to get out at the top. The mass of the sample was recorded every half hour and an ordinary fiber was introduced for comparison. Here, φ is defined as the unit area mass of growth:

$$\varphi = \frac{m - m_0}{S}$$

where m is the current mass, m_0 is the initial mass and S is the area of the sample. As shown in Fig. 6b, the φ value of the untreated fiber had a rapid increase from 0 to 1.5 h, while no discernible changes were observed in the treated fiber. Other treated and untreated fibers showed little obvious growth in the φ value after 1.5 h, indicating that the ordinary fiber was wetted entirely by the dampness, whereas there was little effect on the superhydrophobic fiber (Fig. 6c and d). More importantly, the treated fiber had equal breathability as the untreated did (Video S4†).

4 Conclusion

In conclusion, we have demonstrated a simple, low cost, environmentally friendly method to fabricate absolutely waterborne superamphiphobic coatings using methyltriethoxysilane, fluorinated alkyl silane and a fluorocarbon surfactant. The coating showed an excellent superamphiphobic ability with contact angles of 160°, 153° and 150° and sliding angles of 1°, 4.7° and 6.3° with respect to water, soybean oil and hexadecane. The coating could be applied on various substrates, such as glass, copper foam and polyester fiber, through spraying or dip-coating. Furthermore, after immersing in acid (pH = 1), alkali (pH = 13) and salt (1 mol L^{-1} NaCl), and after treating at 200 °C for 2 h, the coating still maintained its superamphiphobic ability. Additionally, this superamphiphobic coating exhibited prospective performance for anti-fouling, self-cleaning and damp-proof applications.

Conflicts of interest

There are no conflicts to declare.

Acknowledgements

References

1 A. K. Mohanty, M. Misra and L. T. Drzal, *J. Polym. Environ.*, 2002, **10**, 19–26.

2 A. Tuteja, W. Choi, M. L. Ma, J. M. Mabry, S. A. Mazzella, G. C. Rutledge, G. H. McKinley and R. E. Cohen, *Science*, 2007, **318**, 1618–1622.

3 D. Prat, J. Hayler and A. Wells, *Green Chem.*, 2014, **16**, 4546–4551.

4 Y. Lu, S. Sathasivam, J. L. Song, C. R. Crick, C. J. Carmalt and I. P. Parkin, *Science*, 2015, **347**, 1132–1135.

5 X. Deng, L. Mammen, H. J. Butt and D. Vollmer, *Science*, 2012, **335**, 67–70.

6 R. Furstner, W. Barthlott, C. Neinhuis and P. Walzel, *Langmuir*, 2005, **21**, 956–961.

7 G. Wen, X. Y. Gao, P. Tian, L. S. Zhong, Z. L. L. Wang and Z. G. Guo, *Chem. Eng. J.*, 2018, **346**, 94–103.

8 M. J. Kreder, J. Alvarenga, P. Kim and J. Aizenberg, *Nat. Rev. Mater.*, 2016, **1**(1), 15003.

9 L. Mishchenko, B. Hatton, V. Bahadur, J. A. Taylor, T. Krupenkin and J. Aizenberg, *ACS Nano*, 2010, **4**, 7699–7707.

10 L. L. Cao, A. K. Jones, V. K. Sikka, J. Z. Wu and D. Gao, *Langmuir*, 2009, **25**, 12444–12448.

11 P. Guo, Y. M. Zheng, M. X. Wen, C. Song, Y. C. Lin and L. Jiang, *Adv. Mater.*, 2012, **24**, 2642–2648.

12 K. Golovin, S. P. R. Kobaku, D. H. Lee, E. T. DiLoreto, J. M. Mabry and A. Tuteja, *Sci. Adv.*, 2016, **2**(3), e1501496.

13 W. W. Zhang, S. L. Wang, Z. Xiao, X. Q. Yu, C. H. Liang and Y. F. Zhang, *Langmuir*, 2017, **33**, 8891–8898.

14 J. Ou, B. Perot and J. P. Rothstein, *Phys. Fluids*, 2004, **16**, 4635–4643.

15 M. J. Cheng, M. M. Song, H. Y. Dong and F. Shi, *Small*, 2015, **11**, 1665–1671.

16 X. B. Zhang, J. Zhao, Q. Zhu, N. Chen, M. W. Zhang and Q. M. Pan, *ACS Appl. Mater. Interfaces*, 2011, **3**, 2630–2636.

17 P. Calcagnile, D. Fragouli, I. S. Bayer, G. C. Anyfantis, L. Martiradonna, P. D. Cozzoli, R. Cingolani and A. Athanassiou, *ACS Nano*, 2012, **6**, 5413–5419.

18 L. Feng, Z. Y. Zhang, Z. H. Mai, Y. M. Ma, B. Q. Liu, L. Jiang and D. B. Zhu, *Angew. Chem., Int. Ed.*, 2004, **43**, 2012–2014.

19 B. Wang, W. X. Liang, Z. G. Guo and W. M. Liu, *Chem. Soc. Rev.*, 2015, **44**, 336–361.

20 H. Zhu, L. Gao, X. Yu, C. Liang and Y. Zhang, *Appl. Surf. Sci.*, 2017, **407**, 145–155.

21 X. Yin, C. C. Sun, B. Zhang, Y. Z. Song, N. C. Wang, L. P. Zhu and B. K. Zhu, *Chem. Eng. J.*, 2017, **330**, 202–212.

22 T. Gong, J. Kim, J. Y. Woo, J. H. Jang, S. E. Lee and C. S. Han, *RSC Adv.*, 2017, **7**, 25796–25802.

23 Y. M. Zheng, H. Bai, Z. B. Huang, X. L. Tian, F. Q. Nie, Y. Zhao, J. Zhai and L. Jiang, *Nature*, 2010, **463**, 640–643.

24 A. R. Parker and C. R. Lawrence, *Nature*, 2001, **414**, 33–34.

25 M. Wang, Q. Liu, H. Zhang, C. Wang, L. Wang, B. Xiang, Y. Fan, C. F. Guo and S. Ruan, *ACS Appl. Mater. Interfaces*, 2017, **9**, 29248–29254.

26 B. X. Leng, Z. Z. Shao, G. de With and W. H. Ming, *Langmuir*, 2009, **25**, 2456–2460.

27 C. Aulin, S. H. Yun, L. Wagberg and T. Lindstrom, *ACS Appl. Mater. Interfaces*, 2009, **1**, 2443–2452.

28 K. Zhao, K. S. Liu, J. F. Li, W. H. Wang and L. Jiang, *Scr. Mater.*, 2009, **60**, 225–227.

29 H. Zhao, K. Y. Law and V. Sambhy, *Langmuir*, 2011, **27**, 5927–5935.

30 H. Jin, M. Kettunen, A. Laiho, H. Pynnonen, J. Paltakari, A. Marmur, O. Ikkala and R. H. A. Ras, *Langmuir*, 2011, **27**, 1930–1934.

31 A. Susarrey-Arce, A. G. Marin, S. Schlautmann, L. Lefferts, J. G. E. Gardeniers and A. van Houselt, *J. Micromech. Microeng.*, 2012, **23**(2), 025004.

32 D. T. Ge, L. L. Yang, Y. F. Zhang, Y. Rahmawan and S. Yang, *Part. Part. Syst. Charact.*, 2014, **31**, 763–770.

33 H. Zhou, H. Wang, H. Niu, J. Fang, Y. Zhao and T. Lin, *Adv. Mater. Interfaces*, 2015, **2**(6), 1400559.

34 H. Liu, J. Y. Huang, Z. Chen, G. Q. Chen, K. Q. Zhang, S. S. Al-Deyab and Y. K. Lai, *Chem. Eng. J.*, 2017, **330**, 26–35.

35 A. Milionis, K. Dang, M. Prato, E. Loth and I. S. Bayer, *J. Mater. Chem. A*, 2015, **3**, 12880–12889.

36 C. Schlaich, L. Yu, L. Cuellar Camacho, Q. Wei and R. Haag, *Polym. Chem.*, 2016, **7**, 7446–7454.

37 C. Schlaich, L. Cuellar Camacho, L. Yu, K. Achazi, Q. Wei and R. Haag, *ACS Appl. Mater. Interfaces*, 2016, **8**, 29117–29127.